Enhancement of the Electron Spin Resonance of Single-Walled Carbon Nanotubes by Oxygen Removal

William D. Rice,[†,‡] Ralph T. Weber,[§] Ashley D. Leonard,[⊥] James M. Tour,[⊥,∥] Pavel Nikolaev,[¶] Sivaram Arepalli,[¶] Vladimir Berka,[#] Ah-Lim Tsai,[#] and Junichiro Kono[†,‡,*]

[†]Department of Electrical and Computer Engineering and [‡]Department of Physics and Astronomy, Rice University, Houston, Texas 77005, United States, [§]Bruker BioSpin Corporation, Billerica, Massachusetts 01821, United States, [⊥]Department of Chemistry and [∥]Department of Mechanical Engineering and Materials Science, Rice University, Houston, Texas 77005, United States, [¶]Department of Energy Science, Sungkyunkwan University, Suwon 440-746, South Korea, and [#]University of Texas Medical School, Houston, Texas 77030, United States

ABSTRACT

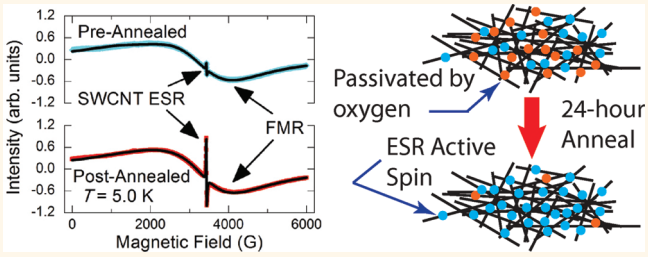

We have observed a nearly 4-fold increase in the electron spin resonance (ESR) signal from an ensemble of single-walled carbon nanotubes (SWCNTs) due to oxygen desorption. By performing temperature-dependent ESR spectroscopy both before and after thermal annealing, we found that the ESR in SWCNTs can be reversibly altered *via* the molecular oxygen content in the samples. Independent of the presence of adsorbed oxygen, a Curie law (spin susceptibility $\propto 1/T$) is seen from ~4 to 300 K, indicating that the probed spins are finite-level species. For both the pre-annealed and post-annealed sample conditions, the ESR line width decreased as the temperature was increased, a phenomenon we identify as motional narrowing. From the temperature dependence of the line width, we extracted an estimate of the intertube hopping energy; for both sample conditions, we found this hopping energy to be ~1.2 meV. Since the spin hopping energy changes only slightly when oxygen is desorbed, we conclude that only the spin susceptibility, not spin transport, is affected by the presence of physisorbed molecular oxygen in SWCNT ensembles. Surprisingly, no line width change is observed when the amount of oxygen in the SWCNT sample is altered, contrary to other carbonaceous systems and certain 1D conducting polymers. We hypothesize that physisorbed molecular oxygen acts as an acceptor (p-type), compensating the donor-like (n-type) defects that are responsible for the ESR signal in bulk SWCNTs.

KEYWORDS: electron spin resonance · single-walled carbon nanotubes · oxygen desorption

One of the most important fields in modern physics is dedicated to understanding spin dynamics in condensed matter systems[1−8] and applied devices.[9,10] Spin transport is a sensitive probe of many-body correlations, as well as an indispensable process for spintronics. When spins are dimensionally confined, especially to one dimension (1D), they are predicted to show strong correlations[3,4,6−8,11] and long coherence times.[5] Single-walled carbon nanotubes (SWCNTs) are ideal materials for studying 1D spin physics due to their long mean free paths and weak spin−orbit coupling.[12] Exotic spin properties in metallic SWCNTs at low temperatures and high magnetic fields have been predicted, including the appearance of a peak splitting in the spin energy density spectrum, which can be used to probe spin−charge separation in Luttinger liquid theory.[6−8]

Despite the predictions of unique and exciting spin-related phenomena, the spin properties of SWCNTs are still poorly understood. One of the most ubiquitous experimental methods for studying spin dynamics, electron spin resonance (ESR) spectroscopy, has been the prime method used to measure the spin dynamics of SWCNTs because it provides information on spin−orbit coupling, phase relaxation time, spin susceptibility, and spin diffusion. However, there are substantial disagreements in the literature on SWCNT ESR line width, spin susceptibility, *g*-factor, and line shape.[13−22] In particular, the temperature dependence of the spin susceptibility of SWCNTs has been surprisingly difficult to reproduce.[15,17,19,22] The experimental evidence is so conflicting that even the origin of the ESR in SWCNTs is under substantial uncertainty, with certain authors claiming it results from defects[14,17,21,23] and others suggesting it is intrinsic to nanotubes.[15,16,19,20,24]

To complicate matters further, adsorbed molecular gas species, such as oxygen and hydrogen, have long been known to strongly affect spins in carbonaceous

* Address correspondence to kono@rice.edu.

Received for review October 24, 2011 and accepted February 12, 2012.

Published online February 12, 2012
10.1021/nn204094s

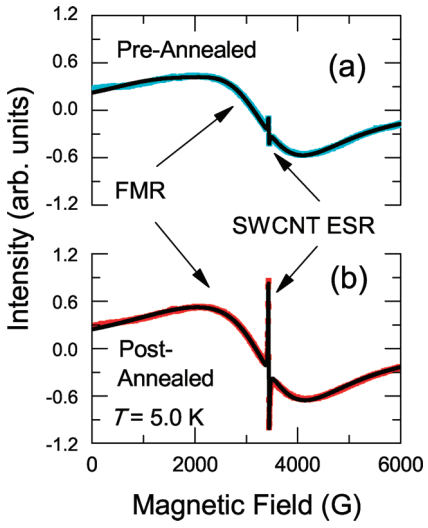

Figure 1. (a) Full range ESR scan at 5.0 K of SWCNT sample before annealing (cyan), where the ESR signal is buried in the large FMR background. (b) Full scan of SWCNT sample at 5.0 K after annealing (red), where the SWCNT ESR is the dominant feature. Black curves indicate fits composed of two large line width Lorentzian lines, which describe the FMR background, and a Dysonian line describing the SWCNT ESR. The FMR intensities stay the same before and after annealing.

systems.[25−31] ESR studies done on adsorbed gas species in carbon nanotubes have focused solely on the adsorption of hydrogen,[23,24,32−34] with only an ambiguous mention of oxygen effects in a polymer−SWCNT film sample.[34] Interestingly, adsorbed hydrogen produces an *increase* in the multiwalled carbon nanotube (MWCNT) ESR, while creating a *decrease* in the ESR signal in SWCNTs.[32,33] These diametrically opposing trends are not currently understood, especially given the fact that the origin of the SWCNT ESR is still under considerable debate. However, many experimental studies have postulated that the signal from MWCNTs occurs from defects,[23,24,32,33] suggesting that hydrogen may not affect the intrinsic nanotube response.

Here, we show that adsorbed molecular oxygen has a considerable influence on the spin susceptibility of SWCNT ensembles, while having only a very small impact on spin movement. By looking at the ESR of SWCNTs as a function of temperature (T) both before (pre-annealed) and after (post-annealed) thermal annealing, we were able to quantitatively evaluate the impact of adsorbed oxygen spins in SWCNTs. Strikingly, we found that oxygen desorption increased the ESR signal by nearly a factor of 4. When oxygen was added back to the system, the ESR signal was once again quenched, indicating reversibility. Despite the change in signal intensity with oxygen, the spin hopping energy stayed around ~1.2 meV for both annealing sample conditions. We hypothesize that the ESR SWCNT signal is due to n-type defects, which are compensated by p-type oxygen acceptor states when present in the sample.

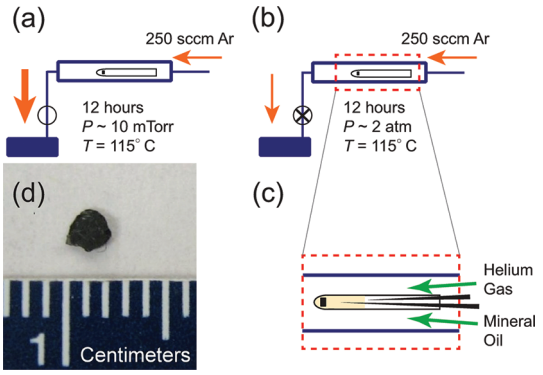

Figure 2. Steps for annealing the sample are given in (a−c). (a) First 12 h anneal stage with T = 115 °C and pressure held at 10 mTorr with a 250 sccm argon flow (argon gas flow indicated by the orange arrows). (b) Second 12 h anneal stage. For this step, we raised the pressure inside the furnace to 2 atm with the vacuum valve held open just enough to keep the pressure steady. (c) To ensure that oxygen did not recontaminate the sample during ESR measurements, we backfilled the ESR tube with degassed mineral oil while streaming helium gas before the sample was removed from the furnace. (d) Picture of the sample before it was placed inside the ESR tube.

The SWCNT sample consisted of acid-purified laser-oven nanotubes obtained from NASA.[35] Despite the soft-bake acid-purification procedure used to remove ferromagnetic catalyst particles (cobalt and nickel), it is evident using ESR spectroscopy that they remain in the sample (Figure 1). We performed both thermogravimetric analysis (TGA) and X-ray photoelectron spectroscopy (XPS) to determine the mass concentration of the metallic catalyst particles. Using XPS, we determined the ratio of the Co to Ni catalyst to be 0.9:1.0, which is very close to the values reported by Nikolaev *et al.*[35] Subsequently, this ratio enables us to compute how much of the resulting oxidized mass produced by TGA (Figure S2 in the Supporting Information) is due to the catalytic metal. For this particular laser-oven sample, we attribute 5.8% of the mass to ferromagnetic catalyst particles. This non-negligible mass percentage explains why the ferromagnetic resonance (FMR) from the catalyst particles dominates the background of the ESR scans of SWCNTs, as seen in Figure 1a.

The SWCNT sample used for ESR measurements was prepared with meticulous attention to compaction and sample homogeneity because small perturbations in the SWCNTs position affect the ESR signal (details presented in the Materials and Methods section). A pictorial scheme, given in Figure 2, shows the steps taken to anneal the sample after it has been created. The powdered SWCNT ensemble was compacted into a pellet and then placed in a desiccator for several days to create a water-free SWCNT pellet; this sample condition is denoted in the text as "pre-annealed". The 0.6 mg (0.38 g/cm^3) SWCNT pellet was then put into a quartz ESR tube and held in place with quartz wool. X-band (9.6 GHz) temperature-dependent ESR

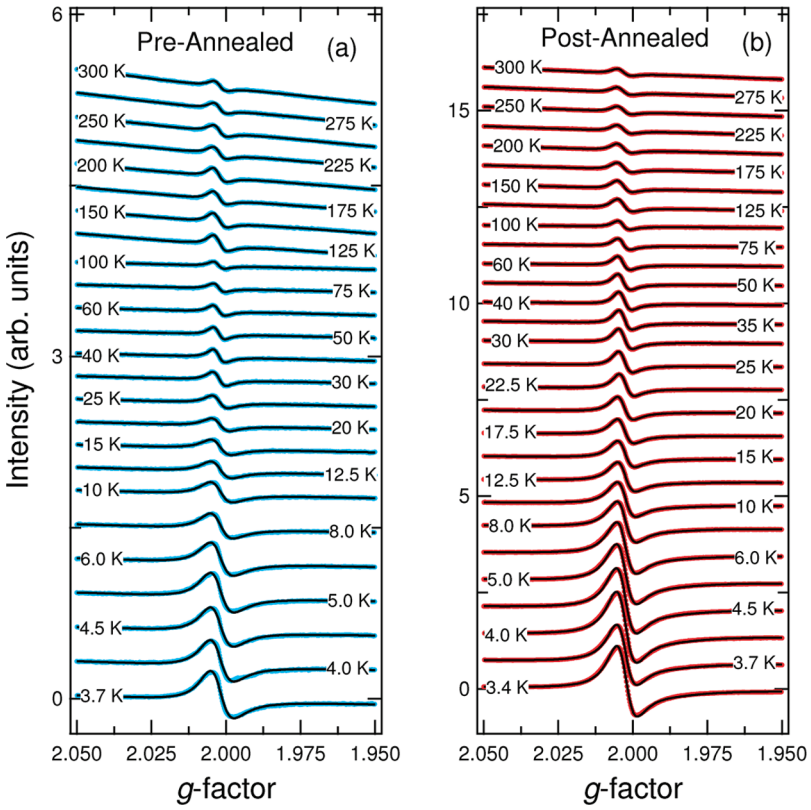

Figure 3. Raw ESR scans of sample (a) before (cyan curves) and (b) after (red curves) annealing as a function of *T*. Black lines indicate fits to the traces.

measurements were taken at discrete temperatures from 3.7 to 300 K. The sample was then brought to a vacuum furnace and annealed at 115 °C for 24 h. After the annealing, the ESR tube was then rigorously prepared to prevent re-exposure to air. In the text, we refer to this sample condition as "post-annealed". As with the pre-annealed sample condition, temperature-dependent ESR scans were performed on the post-annealed sample from 3.4 to 300 K.

RESULTS

Figure 1 shows the remarkable difference that occurs upon thermal annealing: the SWCNT ESR peak goes from being buried in the large catalyst FMR background to dominating the spectrum. Despite the tremendous increase in the SWCNT ESR signal, the FMR hardly changes, demonstrating that the annealing *only* affects the nanotube ESR. The full scan spectra were fit using three curves: two large line width Lorentzians for the two catalyst species, Co and Ni, and a Dysonian line for the SWCNT ESR centered at 3430 G when the microwave frequency is 9.6 GHz.[22] No arbitrary slope or numerical offsets were used in addition to the three lines. The long scan fits, represented by the black curves in Figure 1, describe the observed spin resonance spectrum very well.

A more detailed set of scans covering 2 orders of magnitude in temperature, which are shown in Figure 3, allow a more quantitative understanding of the SWCNT ESR. The raw data traces presented in Figure 3 are fit with a Dysonian line shape (black traces) for each different temperature. The baseline, which becomes more prominent at higher temperatures, is simultaneously fit using two large line width Lorentzians to account for the slowly varying FMR background. The lack of secondary peaks and anomalous shapes, as is seen in other publications,[13,17,21] attests to the purity of our sample. If MWCNTs,[36] amorphous carbon,[37] or graphite[38] contributed to the ESR signal, they would each manifest themselves differently in line shape and as a function of temperature. Therefore, we conclude that we are observing a spin resonance from SWCNTs. Figure 3 shows that, for both sample conditions, the SWCNT ESR increases as *T* decreases. Since the signal intensity is proportional to the mass spin susceptibility, χ_g, the ESR signal change as a function of *T* strongly suggests that we are not observing Pauli law behavior, in which χ_g is independent of *T*. Further, as seen in both Figure 1 and Figure 3, the ESR signal size changes dramatically upon annealing.

To examine these observations more quantitatively, we extracted χ_g from the fitted spectra in Figure 3. We used a $CuSO_4 \cdot 5H_2O$ spin concentration standard measured at temperatures between 4 and 300 K to obtain mass spin susceptibility values from our measurements.

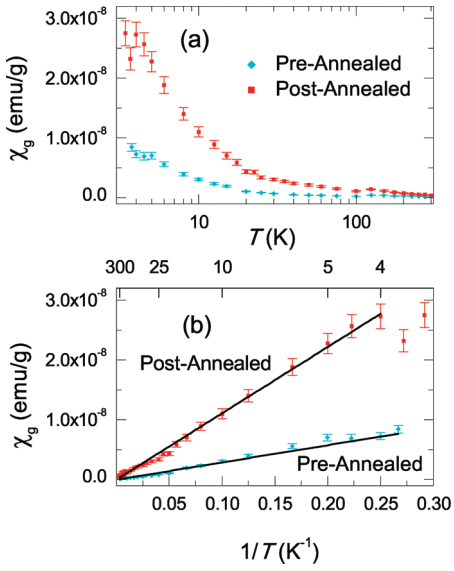

Figure 4. (a) Mass spin susceptibility χ_g as a function of T for the sample before annealing (cyan) and after annealing (red). (b) χ_g *versus* 1/T for the sample before annealing (cyan) and after annealing (red). Annealing produces a large increase in the magnitude of χ_g but does not change its temperature dependence. Both sets of data can be fit well using a Curie law model (black lines) down to ~4 K.

Figure 4 shows how χ_g varies as a function of T for both sample conditions. The large increase in χ_g between the pre-annealed and post-annealed sample conditions is striking, especially at low temperatures. Clearly, the annealing process greatly augments the number of spins probed.

Plotting χ_g *versus* 1/T shows that, for both the pre- and post-annealed sample conditions, the spin susceptibility follows a Curie law behavior:

$$\chi_g = C/T \quad (1)$$

where C is the Curie constant and is equivalent to $(\mu_B^2 N)/(k_B)$, μ_B is the Bohr magneton, N is the number of probed spins, and k_B is the Boltzmann constant. For the pre-annealed sample condition, we fit the values of χ_g from 300 to 3.7 K and find that $C = 2.88 \pm 0.21 \times 10^{-8}$ emu-K/g, which translates into 7.9×10^{12} spins. This value for the pre-annealed Curie constant is very close to what Likodimos *et al.* found in their work,[19] as well as what other groups have estimated their mass susceptibility to be.[17,18] Similarly, if we fit the post-annealed data from 300 to 4.0 K, we extract $C = 1.11 \pm 0.04 \times 10^{-7}$ emu-K/g (3.0×10^{13} spins). Therefore, by removing adsorbed gases from the SWCNTs, the number of spins probed is increased by a factor of 3.9. Interestingly, both pre-annealed and post-annealed sample conditions show Curie law trends down to ~4 K. However, as the temperature drops below 4 K, χ_g seems to deviate from eq 1, especially for the post-annealed sample; further investigation is needed to determine how χ_g varies with T at temperatures below 4 K.

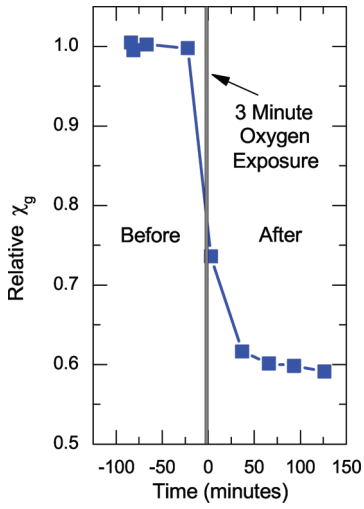

Figure 5. Relative spin susceptibility of an annealed SWCNT sample over several hours shows a sudden decrease once oxygen is introduced (gray shaded region). After nearly 2 h, the decrease in spin susceptibility appears to stop, indicating that equilibrium has been reached.

To investigate which adsorbed gas species might contribute to this marked rise in the spin susceptibility, we applied a constant pressure of pure oxygen onto a freshly annealed powdered SWCNT sample. Immediately after the oxygen exposure, we ran an ESR scan to interrogate how the sample responded to the presence of oxygen. We repeated the ESR scans every 30 min to see how the signal evolved (details given in the Supporting Information). As Figure 5 shows, the relative spin susceptibility dramatically decreases as the oxygen is adsorbed onto the SWCNTs, dropping to 59% of the initial annealed spin susceptibility. As a comparison, the ratio of the pre-annealed spin susceptibility to the post-annealed spin susceptibility at T = 300 K is 0.42. The fact that the presence of oxygen does not fully return the ESR to its original suppressed value may be due to the inability of the oxygen to return to its former locations between SWCNTs. Once the oxygen is removed, the strong van der Waals forces between tubes reduce the intertube spacing, thus preventing oxygen from quenching the ESR. This test unequivocally shows that oxygen is a strong spin suppressor in SWCNTs. Importantly, Figure 5 demonstrates that the annealing effect is *reversible*: we can remove molecular oxygen and increase χ_g and then add molecular oxygen back to the system and suppress χ_g.

DISCUSSION

In addition to the ESR signal size decreasing as T increases, the half-width at half-maximum of the line, ΔH, becomes smaller as T is raised, as seen in Figure 3. This phenomenon, which we have previously reported,[22] is known as motional narrowing:[39,40] it occurs because the dephasing time of the spins changes as their translational energy is altered. At high T, the spins move rapidly, allowing for less time around

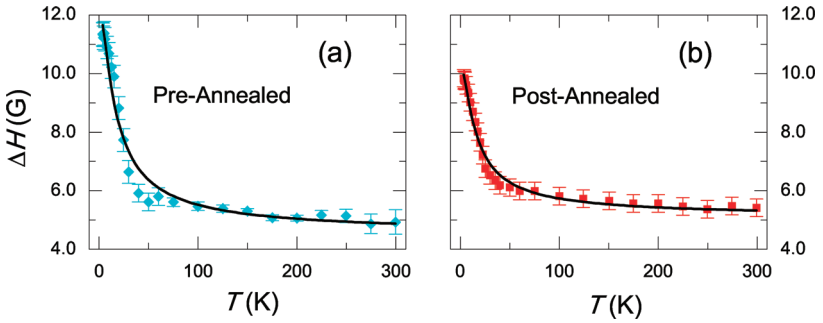

Figure 6. ESR line width *versus* *T* for the (a) pre-annealed and (b) post-annealed sample conditions. The black lines indicate the fitting of eq 2 to the data.

dephasing centers, thus reducing the interaction between the probed spins and the dephasing centers. This decreased interaction gives a longer spin dephasing time (T_2), which in turn narrows the line. Conversely, at low T, the spins are moving more slowly, which broadens the line. Interestingly, we observe that this behavior occurs for both the annealed and non-annealed sample conditions.

We can see the phenomenon of motional narrowing more clearly in Figure 6. The exponential decrease in ΔH is well described by combining Anderson's motional narrowing relation with a hopping wave function to model the spin movement:[22,41−44]

$$\Delta H = \Delta H_0 + \frac{A}{\Delta E \times \left[1 + \coth\left(\frac{\Delta E}{2k_B T}\right)\right]} \quad (2)$$

where ΔH_0 is the high-T ("metallic") limit of the line width, A is a temperature-independent variable, and ΔE is the energy required to move from one location to another. For the pre-annealed sample condition, we extract a ΔH_0 of 4.53 ± 0.10 G ($T_2 = (\hbar/g\mu_B)(1/\Delta H)$ = 12.5 ns) with a hopping energy of 1.26 ± 0.16 meV (T_{hop} = 14.6 K) and A = 18.3 ± 1.9 meV-G. Similarly, we fit the line width temperature dependence for the post-annealed sample condition to obtain A = 11.6 ± 0.8 meV-G and ΔH_0 = 5.10 ± 0.08 G, with the latter quantity giving a T_2 spin dephasing time of 11.1 ns. The activation energy for the post-annealed sample condition, ΔE, is 1.18 ± 0.09 meV (13.7 K).

Quantitatively, the annealing procedure seems to have only a minor effect on the hopping energy, changing T_{hop} from 14.6 to 13.7 K. This small change in the hopping characteristics suggests that adsorbed gases have little effect on the motion of the spins. In a similar manner, annealing has a small effect on the line width in the high-T limit, ΔH_0. Annealing increases ΔH_0 by ∼0.5 G, which correspondingly changes the spin dephasing rate, T_2, from 12.5 to 11.1 ns, a relatively small drop. As with the hopping energy, the fact that annealing has only a minor effect on ΔH_0 indicates that adsorbed gases in bulk SWCNT systems have little impact on the mobility of the probed spins.

The fitting of eq 2 to the line width fundamentally captures the narrowing behavior of ΔH as a function of T. As previously mentioned, eq 2 was derived from a hopping motion wave function, which was used to describe motional narrowing in doped semiconductors. Indeed, researchers investigated a similar line width behavior in P-doped Si[45,46] and Ge[43,44] as we observe in SWCNTs. In these doped semiconductor systems, the concentration of the ESR-active defects determines the line shape form and its temperature dependence.[46,47] At low to intermediate donor densities, motional narrowing is expected in these systems because the donor center-to-center distance is smaller than the spatial extent of the spin wave function. Similarly, we found in a previous publication[22] that the spin−spin distance for the post-annealed sample condition is ∼28 nm, while the spin localization length is ∼100 nm. As such, our observation of motional narrowing makes sense, especially if we consider the ESR signal to arise from defects in SWCNTs. Other models, such as those used to examine the line width in 1D conducting polymers,[48,49] may also be good fits, but there, a fundamentally different spin behavior would be assumed. More knowledge about spin diffusion in SWCNTs and how defect concentration changes temperature-dependent ESR is needed to more completely determine the SWCNT line width temperature dependence.

As mentioned above, the mobility of the spins is marginally influenced by the presence of adsorbed gases; rather, it seems to be strongly dependent on the sample temperature, as seen in Figure 6. The center position of the resonance, H_0, on the other hand, is only slightly dependent on the temperature (Figure 7). As is typical in magnetic resonance experiments, we define the g-factor as the ratio of the perturbing field energy to the magnetic dipole energy $g = (h\nu_0)/(\mu_B H_0)$, where h is Planck's constant and ν_0 is the frequency of the perturbing microwave field. The measured g-factor for the pre-annealed sample condition is nearly temperature-independent, staying close to the free electron g-factor value of 2.0023 throughout the full 3.7 to 300 K temperature range. This behavior is similar to the temperature dependence of the g-factor of graphite

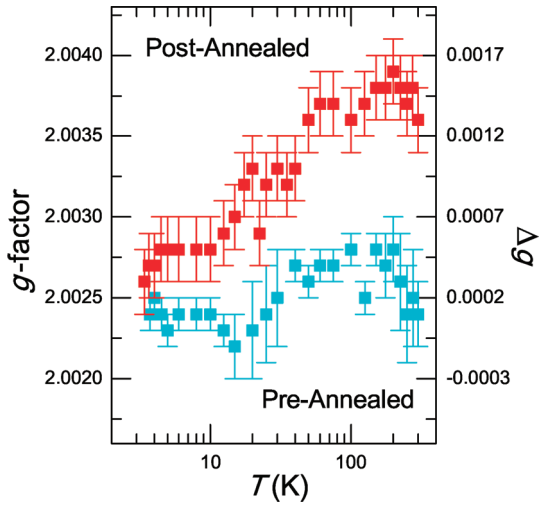

Figure 7. Experimentally obtained *g*-factor values as a function of *T* for the sample before (cyan) and after (red) annealing.

in the plane perpendicular to the *c*-axis.[38,50] The *g*-factor of the post-annealed sample condition shows a slight increase with increasing temperature. However, there is a small, but measurable, change in the *g*-factor upon annealing, especially at high temperatures. If we take g_0 to be the free electron *g*-factor (2.0023), we can define the quantity $\Delta g \equiv g - g_0$. Following Platzman,[51] we interpret Δg to be proportional to the spin−orbit coupling. As such, the upward shift (Δg changes by ~0.001 at T = 300 K) in the *g*-factor upon annealing indicates that adsorbed gas species weakly quench some of the spin−orbit coupling of the probed spins.

As Figure 5 shows, the quenching of the spin susceptibility is reversible when molecular oxygen is introduced. Given this information, as well as the fact we are using a low annealing temperature of 115 °C (33 meV) to create the changes in χ_g, it seems most likely that the spin susceptibility change is caused by physisorbed molecular oxygen; that is, no change in the chemical bonds of the system occurs when oxygen is either added or removed. Indeed, this line of reasoning follows Ulbricht *et al.*, who showed that molecular oxygen primarily physisorbs to SWCNTs[52] (unlike reactive atomic oxygen, which is known to form epoxies and ethers in SWCNTs[53]). In addition, theoretical work has also shown that molecular oxygen should physisorb to SWCNTs.[54−56]

Taken as a whole, our results show that molecular oxygen physisorbed onto SWCNTs affects only χ_g, with minimal changes to ΔH and the *g*-factor. The lack of change in ΔH is especially odd since, in many biological systems, O_2 serves as general relaxer for various paramagnetic species *via* spin−spin interaction, which leads to ESR line broadening. This very nature finds wide application of oxygen in membrane topology studies of membrane-bound macromolecules[57,58] and serves as the theoretical basis for oximetry in quantifying O_2 in a particular biological sample present in aqueous environment.[59] Furthermore, the observation that oxygen does not affect the observed ΔH in SWCNTs also contrasts with previous ESR stuides on gas adsorption in 1D polymer systems, such as *trans*-polyacetylene, which show that ΔH increases as the number of gas molecules (pressure) increases. For example, Houzé and Nechtschein[60] show that exchange and dipolar interactions resulting from an adsorbed gas species broaden the ESR line width, $\Delta\omega$, with the relation given as $\delta(\Delta\omega) = p\omega_{hop}C_i$. Here, p is the probability of a spin flip due to an interaction, ω_{hop} is the hopping frequency of the probed spin species, and C_i is the concentration of the adsorbed gas. If this type of process was occurring in our system, we should see some change in ΔH ($\Delta H = (\hbar\Delta\omega)/(g\mu_B)$) when the oxygen is desorbed (annealing) or adsorbed (oxygen exposure test); however, no significant change in ΔH is observed.

A very fast relaxation process (such as dipolar broadening due to the triplet state of oxygen) could exist in our system. Presumably, this latent ESR signal would show up as a change in the baseline, assuming that the resonance width was on the order of 100 to 1000 G. However, this "spin segregation" into two different relaxation processes seems unlikely, especially since the baseline changes only slightly when the system is exposed to oxygen (see Figure S3 in the Supporting Information). However, given our scan range and signal-to-noise limits, measuring a signal with such a wide line width is difficult. Experiments in the time domain may be necessary to fully support our hypothesis that a very fast relaxing spin from the SWCNTs does not exist.

A more plausible hypothesis is that oxygen is passivating the paramagnetic moments of SWCNT defects. These defects could be caused during SWCNT growth, processing, or even acid purification.[35] As shown in the discrete Raman spectroscopy plot in the Supporting Information (Figure S1), we have a measurable amount of lattice defects, so an ESR signal from, say, topological defects or dangling bonds is possible. Despite the localized nature of the ESR-active species, the unpaired electrons still have mobility in this scenario: the Dysonian signal in our work does not come from conduction electrons, as with ESR from bulk metals, but from thermally activated finite-level species. In addition, if we were probing defects or dangling bonds, we would expect both a Curie law spin susceptibility temperature dependence, as well as a *g*-factor that is close to the free electron value; we observe both behaviors in our system. Additionally, ESR arising from nonpristine SWCNTs would explain why the tremendous variation in ESR signals exists in the literature: in essence, different SWCNT purification methods and sample preparation steps would create differing resonance signals.

We can quantify how prevalent these ESR-active defects are by using the extracted estimate for the Curie coefficient of the post-annealed sample ($1.11 \pm 0.04 \times 10^{-7}$ emu-K/g). If we assume that all of the SWCNTs in our sample are (10,10) nanotubes, we find that there is roughly one probed spin for every 3×10^5 carbon atoms. Though this number in itself may not establish that the ESR signal arises from nonpristine SWCNTs, it does suggest an exceedingly weak response (assuming a SWCNT length of 1 μm, $C = 3.60 \times 10^{-25}$ emu-K/SWCNT).

The quenching of the signal from oxygen exposure may result from a compensation mechanism. If, for example, the defects responsible for the ESR signal are n-type, creating states closer to the conduction band edge within the band gap, then they can be compensated by the introduction of acceptors. Oxygen is thought to be a p-type acceptor to SWCNT, especially in the presence of defects.[61,62] If the oxygen molecule is in the spin-singlet state, even charge transfer (chemisorption) can occur.[61−63] The adsorption of oxygen molecules to the ESR-active defects would suppress the ESR signal; subtracting weakly bound oxygen from the system would reverse this quench. A parametric study of ESR as a function of oxygen pressure is needed to further clarify our observations, including the exact nature of the defects.

CONCLUSION

In conclusion, we have clearly demonstrated that spin susceptibility in nanotubes is strongly influenced by the presence of physisorbed oxygen. We observe a nearly 4-fold increase in spin susceptibility by desorbing gases present in our SWCNT ensemble. The presence of adsorbed gases is shown not to substantially affect the spin hopping energy, which we find to be ~1.2 meV. We observe that the *g*-factor is very close to the free electron value for both the pre-annealed and post-annealed sample conditions. The decrease of the *g*-factor with decreasing temperature is not well-explained. We hypothesize that the spin suppression is due to compensation of donor-type defects by acceptor oxygen states.

MATERIALS AND METHODS

The sample consisted of acid-purified laser-oven SWCNTs obtained from NASA.[35] We used extreme care to prepare the SWCNT sample for ESR measurements because both compaction density and particle looseness have an effect on the ESR signal. The powdered SWCNT ensemble was gently bath sonicated (Cole-Parmer, model B3-R) at 12 W and a frequency of 55 kHz. Sonication lasted for 2 h in water before the mixture was ultracentrifuged at 26 000 rpm (an average force of 88 000*g* using a Sorvall AH-629 rotor with 36 mL centrifuge tubes) for 4 h. After ultracentrifugation, the supernatant was removed, and the resulting SWCNT pellet was extracted from the centrifuge tube and placed into an open-air oven at 115 °C for 15 min to remove most of the water. At this point, the pellet was dry enough to be handled as a solid unit. It was then placed into a desiccator for several days to create a water-free SWCNT pellet; this sample condition is denoted in the text as "pre-annealed". The 0.6 mg (0.38 g/cm^3) SWCNT pellet was held in a 3 mm diameter quartz ESR tube using quartz wool.

The sample was then placed into a vacuum furnace kept at 115 °C for 24 h. For the first 12 h, the pressure inside the furnace was maintained at 10 mTorr vacuum with a 250 sccm flow of purified argon; for the last 12 h, the argon pressure was increased to ≈2 atm pressure with a 250 sccm argon flow. After the annealing, the ESR tube was partially filled with degassed mineral oil; the mechanical integrity of the pellet was completely preserved despite the addition of the mineral oil. While the mineral oil was being inserted into the ESR tube, a helium gas flow was simultaneously being applied so as to create a positively pressurized helium blanket. Both the mineral oil and the gas were introduced into the ESR tube while it lay in the furnace using 12 in. syringes. Helium gas was blanketed on top of the mineral oil before the ESR tube was mechanically sealed to prevent exposure to air. In the text, we refer to this sample condition as "post-annealed".

Temperature-dependent ESR measurements of the pellet were taken at discrete temperatures from ~3 to 300 K using a Bruker EMX X-band (9.6 GHz) spectrometer. An Oxford ESP900 cryostat with a ITC503 temperature controller and GFS600 transfer line was used for temperatures from 3.4 to 100 K, and a BVT3000 temperature controller with a silver-coated double-jacketed glass transfer line was used for temperatures above 100 K. From 3 to 100 K, 200 μW of microwave power was applied to the cavity; above 100 K, a microwave power of 1 mW was used. To ensure that we were in the linear power regime, we performed power dependence from 6 μW to 200 mW at temperatures from 4 to 100 K and from 50 μW to 200 mW at temperatures from 125 to 300 K. The ESR signal was not saturated until the power exceeded 10 mW, ensuring the measurements were performed within the linear regime. In addition, we extract estimates of our measurement error from fitting results performed on spectra in the linear regime.

A 2,2-diphenyl-1-picrylhydrazyl (DPPH) standard was used to calibrate the field. We used a 1 mM $CuSO_4 \cdot 5H_2O$ solution as a spin concentration standard to extract a numerical estimate of χ_g; its ESR signal was measured at numerous temperatures from 4 to 300 K. We placed the standard in the same configuration as the SWCNT sample with approximately the same microwave cavity volume to minimize differences between the sample and reference.

Conflict of Interest: The authors declare no competing financial interest.

Acknowledgment. This work was supported by the DOE/BES through Grant No. DEFG02-06ER46308 and DEFC-36-05GO15073, the Robert A. Welch Foundation through Grant No. C-1509, the Air Force Research Laboratories under contract number FA8650-05-D-5807, the W.M. Keck Program in Quantum Materials at Rice University, the NIH National Heart, Lung, and Blood Institute through Grant No. HL095820, and Korean Ministry of Education, Science and Technology under the World Class University Program (R31-2008-10029). We thank Qimiao Si, Adilet Imambekov, and Robert Hauge for useful discussions.

Supporting Information Available: Detailed sample characterization data and further information on the analysis and experimental methods are available in the Supporting Information. This material is available free of charge *via* the Internet at http://pubs.acs.org.

REFERENCES AND NOTES

1. Si, Q. Spin Conductivity and Spin-Charge Separation in the High-T_c Cuprates. *Phys. Rev. Lett.* **1997**, *78*, 1767–1770.
2. Si, Q. Spin Injection into a Luttinger Liquid. *Phys. Rev. Lett.* **1998**, *81*, 3191–3194.
3. Balents, L.; Egger, R. Spin Transport in Interacting Quantum Wires and Carbon Nanotubes. *Phys. Rev. Lett.* **2000**, *85*, 3464–3467.
4. Balents, L.; Egger, R. Spin-Dependent Transport in a Luttinger Liquid. *Phys. Rev. B* **2001**, *64*, 035310.
5. Kiselev, A. A.; Kim, K. W. Progressive Suppression of Spin Relaxation in Two-Dimensional Channels of Finite Width. *Phys. Rev. B* **2000**, *61*, 13115–13120.
6. Rabello, S.; Si, Q. Spectral Functions in a Magnetic Field as a Probe of Spin-Charge Separation in a Luttinger Liquid. *Europhys. Lett.* **2002**, *60*, 882.
7. Martino, A. D.; Egger, R.; Hallberg, K.; Balseiro, C. A. Spin−Orbit Coupling and Electron Spin Resonance Theory for Carbon Nanotubes. *Phys. Rev. Lett.* **2002**, *88*, 206402.
8. Dóra, B.; Gulácsi, M.; Koltai, J.; Zólyomi, V.; Kürti, J.; Simon, F. Electron Spin Resonance Signal of Luttinger Liquids and Single-Wall Carbon Nanotubes. *Phys. Rev. Lett.* **2008**, *101*, 106408.
9. DiVincenzo, D. P. Quantum Computation. *Science* **1995**, *270*, 255.
10. Wolf, S. A.; Awschalom, D. D.; Buhrman, R. A.; Daughton, J. M.; von Molnar, S.; Roukes, M. L.; Chtchelkanova, A. Y.; Treger, D. M. Spintronics: A Spin-Based Electronics Vision for the Future. *Science* **2001**, *294*, 1488–1495.
11. Giamarchi, T. *Quantum Physics in One Dimension*; Oxford University Press: Oxford, 2004.
12. Ando, T. Spin−Orbit Interaction in Carbon Nanotubes. *J. Phys. Soc. Jpn.* **2000**, *69*, 1757–1763.
13. Kosaka, M.; Ebbesen, T. W.; Hiura, H.; Tanigaki, K. Electron Spin Resonance of Carbon Nanotubes. *Chem. Phys. Lett.* **1994**, *225*, 161–164.
14. Kosaka, M.; Ebbesen, T. W.; Hiura, H.; Tanigaki, K. Annealing Effect on Carbon Nanotubes. *Chem. Phys. Lett.* **1995**, *233*, 47–51.
15. Petit, P.; Jouguelet, E.; Fischer, J. E.; Rinzler, A. G.; Smalley, R. E. Electron Spin Resonance and Microwave Resistivity of Single-Wall Carbon Nanotubes. *Phys. Rev. B* **1997**, *56*, 9275–9278.
16. Claye, A. S.; Nemes, N. M.; Jánossy, A.; Fischer, J. E. Structure and Electronic Properties of Potassium-Doped Single-Wall Carbon Nanotubes. *Phys. Rev. B* **2000**, *62*, R4845–R4848.
17. Salvetat, J.-P.; Fehér, T.; L'Huillier, C.; Beuneu, F.; Forró, L. Anomalous Electron Spin Resonance Behavior of Single-Wall Carbon Nanotubes. *Phys. Rev. B* **2005**, *72*, 075440.
18. Náfrádi, B.; Nemes, N. M.; Fehér, T.; Forró, L.; Kim, Y.; Fischer, J. E.; Luzzi, D. E.; Simon, F.; Kuzmany, H. Electron Spin Resonance of Single-Walled Carbon Nanotubes and Related Structures. *Phys. Status Solidi B* **2006**, *243*, 3106–3110.
19. Likodimos, V.; Glenis, S.; Guskos, N.; Lin, C. L. Antiferromagnetic Behavior in Single-Wall Carbon Nanotubes. *Phys. Rev. B* **2007**, *76*, 075420.
20. Corzilius, B.; Dinse, K.-P.; Hata, K.; Haluška, M.; Skákalová, V.; Roth, S. SWNT Probed by Multi-Frequency EPR and Non-resonant Microwave Absorption. *Phys. Status Solidi B* **2008**, *245*, 2251–2254.
21. Ferrer-Anglada, N.; Monge, A. A.; Roth, S. Electron Spin Resonance on Single-Walled Carbon Nanotubes Obtained from Different Sources. *Phys. Status Solidi B* **2010**, *247*, 2823–2826.
22. Rice, W. D.; Weber, R. T.; Nanot, S.; Nikolaev, P.; Arepalli, S.; Tsai, A.-L.; Kono, J. Motional Narrowing of Electron Spin Resonance in Single-Walled Carbon Nanotubes. arXiv:1105.5095v2 [cond-mat.mes-hall] **2011**.
23. Musso, S.; Porro, S.; Rovere, M.; Tagliaferro, A.; Laurenti, E.; Mann, M.; Teo, K. B. K.; Milne, W. I. Low Temperature Electron Spin Resonance Investigation on SWNTs after Hydrogen Treatment. *Diamond Relat. Mater.* **2006**, *15*, 1085–1089.
24. Kombarakkaran, J.; Pietrass, T. Electron Spin Resonance Studies of Hydrogen Adsorption on Single-Walled Carbon Nanotubes. *Chem. Phys. Lett.* **2008**, *452*, 152–155.
25. Pastor, R. C.; Weil, J. A.; Brown, T. H.; Turkevich, J. Narrow Electron Spin Resonance in Charred Dextrose. *Phys. Rev.* **1956**, *102*, 918–919.
26. Arnold, G. M. A Survey of ESR in Heat Treated Carbon Blacks. *Carbon* **1957**, *5*, 33–42.
27. Singer, L. S.; Lewis, I. C. Applications of ESR to Carbonaceous Materials. *Appl. Spectrosc.* **1982**, *36*, 52–57.
28. di Vittorio, S. L.; Nakayama, A.; Enoki, T.; Dresselhaus, M. S.; Endo, M.; Shindo, N. ESR Study of Activated Carbon Fibers: Preliminary Results. *J. Mater. Res.* **1993**, *8*, 2282–2287.
29. Atsarkin, V. A.; Demidov, V. V.; Vasneva, G. A.; Dzheparov, F. S.; Ceroke, P. J.; Odintsov, B. M.; Clarkson, R. B. Mechanism of Oxygen Response in Carbon-Based Sensors. *J. Magn. Reson.* **2001**, *149*, 85–89.
30. von Bardeleben, H. J.; Cantin, J. L.; Zellama, K.; Zeinert, A. Spins and Microstructures of Amorphous Carbon. *Diamond Relat. Mater.* **2003**, *12*, 124–129.
31. Rao, S. S.; Stesmans, A.; Keunen, K.; Kosynkin, D. V.; Higginbotham, A.; Tour, J. M. Unzipped Graphene Nanoribbons as Sensitive O_2 Sensors: Electron Spin Resonance Probing and Dissociation Kinetics. *Appl. Phys. Lett.* **2011**, *98*, 083116.
32. Shen, K.; Tierney, D. L.; Pietrass, T. Electron Spin Resonance of Carbon Nanotubes under Hydrogen Adsorption. *Phys. Rev. B* **2003**, *68*, 165418.
33. Clewett, C. F. M.; Kombarakkaran, J.; Pietrass, T. ESR Studies of Gas Adsorption on Carbon Nanotubes. *Phys. Status Solidi B* **2006**, *243*, 3242–3245.
34. Konchits, A. A.; Kolesnik, S. P.; Yefanov, V. S.; Motsnyi, F. V.; Tamburri, E.; Terranova, M.-L. ESR Study of Hydrogen Sorption/Desorption Kinetics in Poly(*ortho*-anisidine) and POA/SWNTs Composite Films. In *Carbon Nanomaterials in Clean Energy Hydrogen Systems*; Springer: Dordrecht, The Netherlands, 2008; pp 241−250.
35. Nikolaev, P.; Gorelik, O.; Allada, R.; Sosa, E.; Arepalli, S.; Yowell, L. Soft-Bake Purification of Single-Walled Carbon Nanotubes Produced by Pulsed Laser Vaporization. *J. Phys. Chem. C* **2007**, *111*, 17678–17683.
36. Beuneu, F.; L'Huillier, C.; Salvetat, J.-P.; Bonard, J.-M.; Forró, L. Modification of Multiwall Carbon Nanotubes by Electron Irradiation: An ESR Study. *Phys. Rev. B* **1999**, *59*, 5945–5949.
37. Demichelis, F.; Martino, C. D.; Tagliaferro, A.; Fanciulli, M. Temperature Dependence Analysis of the Electron Paramagnetic Resonance Signal and Electrical Conductivity in a-C and a-C:H. *Diamond Relat. Mater.* **1994**, *3*, 844–848.
38. Wagoner, G. Spin Resonance of Charge Carriers in Graphite. *Phys. Rev.* **1960**, *118*, 647–653.
39. Bloembergen, N.; Purcell, E. M.; Pound, R. V. Relaxation Effects in Nuclear Magnetic Resonance Absorption. *Phys. Rev.* **1948**, *73*, 679–712.
40. Kubo, R.; Tomita, K. A General Theory of Magnetic Resonance Absorption. *J. Phys. Soc. Jpn.* **1954**, *9*, 888–919.
41. Anderson, P. W.; Weiss, P. R. Exchange Narrowing in Paramagnetic Resonance. *Rev. Mod. Phys.* **1953**, *25*, 269–276.
42. Anderson, P. W. A Mathematical Model for the Narrowing of Spectral Lines by Exchange or Motion. *J. Phys. Soc. Jpn.* **1954**, *9*, 316–339.
43. Wilson, D. K. Electron Spin Resonance Experiments on Shallow Donors in Germanium. *Phys. Rev.* **1964**, *134*, A265–A286.
44. Morigaki, K.; Mitsuma, T. Electron Spin Resonance and Relaxation Effects on Donors in Stressed Ge. *J. Phys. Soc. Jpn.* **1965**, *20*, 62–76.
45. Feher, G. Electron Spin Resonance Experiments on Donors in Silicon. I. Electronic Structure of Donors by the Electron Nuclear Double Resonance Technique. *Phys. Rev.* **1959**, *114*, 1219–1244.
46. Maekawa, S.; Kinoshita, N. Electron Spin Resonance in Phosphorus Doped Silicon at Low Temperatures. *J. Phys. Soc. Jpn.* **1965**, *20*, 1447–1457.

47. Ochiai, Y.; Matsuura, E. ESR in Heavily Doped *n*-Type Silicon near a Metal−Nonmetal Transition. *Phys. Status Solidi A* **1976**, *38*, 243–252.
48. Nechtschein, M.; Devreux, F.; Genoud, F.; Guglielmi, M.; Holczer, K. Magnetic-Resonance Studies in Undoped *trans*-Polyacetylene $(CH)_x$. II. *Phys. Rev. B* **1983**, *27*, 61–78.
49. Mizoguchi, K.; Masubuchi, S.; Kume, K.; Akagi, K.; Shirakawa, H. Analysis of the ESR Linewidth in Pristine *trans*-Polyacetylene. *Phys. Rev. B* **1995**, *51*, 8864–8873.
50. Matsubara, K.; Tsuzuku, T.; Sugihara, K. Electron Spin Resonance in Graphite. *Phys. Rev. B* **1991**, *44*, 11845–11851.
51. Platzman, P. M.; Wolff, P. A. *Waves and Interactions in Solid State Plasmas*, 1st ed.; Academic Press: New York, 1973; pp 204−227.
52. Ulbricht, H.; Moos, G.; Hertel, T. Physisorption of Molecular Oxygen on Single-Wall Carbon Nanotube Bundles and Graphite. *Phys. Rev. B* **2002**, *66*, 075404.
53. Larciprete, R.; Gardonio, S.; Petaccia, L.; Lizzit, S. Atomic Oxygen Functionalization of Double Walled Carbon Nanotubes. *Carbon* **2009**, *47*, 2579–2589.
54. Giannozzi, P.; Car, R.; Scoles, G. Oxygen Adsorption on Graphite and Nanotubes. *J. Chem. Phys.* **2003**, *118*, 1003–1006.
55. Dag, S.; Gülseren, O.; Ciraci, S. A Comparative Study of O_2 Adsorbed Carbon Nanotubes. *Chem. Phys. Lett.* **2003**, *380*, 1–5.
56. Dag, S.; Gülseren, O.; Yildirim, T.; Ciraci, S. Oxygenation of Carbon Nanotubes: Atomic Structure, Energetics, and Electronic structure. *Phys. Rev. B* **2003**, *67*, 165424.
57. Millhauser, G. L.; Fiori, W. R.; Miick, S. M. Electron Spin Labels. *Methods Enzymol.* **1995**, *246*, 589–610.
58. Malmberg, N. J.; Buskirk, D. R. V.; Falke, J. J. Membrane-Docking Loops of the cPLA2 C2 Domain: Detailed Structural Analysis of the Protein−Membrane Interface *via* Site-Directed Spin-Labeling. *Biochemistry* **2003**, *42*, 13227–13240.
59. Ahmad, R.; Kuppusamy, P. Theory, Instrumentation, and Applications of Electron Paramagnetic Resonance Oximetry. *Chem. Rev.* **2010**, *110*, 3212–3236.
60. Houzé, E.; Nechtschein, M. ESR in Conducting Polymers: Oxygen-Induced Contribution to the Linewidth. *Phys. Rev. B* **1996**, *53*, 14309–14318.
61. Grujicica, M.; Caoa, G.; Singh, R. The Effect of Topological Defects and Oxygen Adsorption on the Electronic Transport Properties of Single-Walled Carbon-Nanotubes. *Appl. Surf. Sci.* **2003**, *211*, 166–183.
62. Savage, T.; Bhattacharya, S.; Sadanadan, B.; Gaillard, J.; Tritt, T. M.; Sun, Y.-P.; Wu, Y.; Nayak, S.; Car, R.; Marzari, N.; *et al.* Photoinduced Oxidation of Carbon Nanotubes. *J. Phys.: Condens. Matter* **2003**, *15*, 5915–5921.
63. Jhi, S.-H.; Louie, S. G.; Cohen, L. M. Electronic Properties of Oxidized Carbon Nanotubes. *Phys. Rev. Lett.* **2000**, *85*, 1710–1713.